

Saccharide Clusters

How to cite:

International Edition: doi.org/10.1002/anie.202102547

German Edition: doi.org/10.1002/ange.202102547

An Aromatic Micelle-Based Saccharide Cluster with Changeable Fluorescent Color and its Protein Interactions

Haruna Narita, Lorenzo Catti, and Michito Yoshizawa*

Abstract: To develop a new type of synthetic saccharide clusters with changeable fluorescent colors, we herein designed a multisaccharide-coated aromatic micelle. The new cluster forms in water through the quantitative assembly of bent polyaromatic amphiphiles bearing three mannose groups. The spherical assembly, with a 2 nm-sized polyaromatic core and ca. 18 saccharide pendants, is stable even under high dilution conditions (up to 0.02 mM). The emission intensity and color of the saccharide cluster can be altered from moderate blue ($\Phi_F = 19\%$) to strong red, orange, and green (Φ_F up to 67%) upon encapsulation of hydrophobic fluorescent dyes in water. Moreover, the present fluorescent clusters, both with and without the dyes, display selective interactions with mannose-binding proteins *in vitro*.

Saccharide clusters are essential bioarchitectures capable of interacting with protein surfaces with high specificity.^[1,2] The majority of natural clusters possess relatively large and complex multisaccharide frameworks so that their total syntheses remain difficult. From the viewpoints of basic biochemical research and medical applications, several types of synthetic saccharide clusters have been developed, such as (i) covalent dendrimer-shaped and macrocycle-based clusters,^[3,4] (ii) metal nanoparticle-based clusters,^[5] (iii) non-covalent micellar and vesicle-like clusters,^[6,7] and (iv) metal-organic framework (MOF)-type clusters (Figure 1 a–d).^[8] The attachment and incorporation of fluorophores within the clusters have been demonstrated to provide clusters with photofunctions.^[9] However, both covalent as well as non-covalent saccharide clusters displaying high emissivity with various emission colors are scarcely reported so far, owing to aggregation-caused quenching (ACQ) or the heavy metal effect.^[10] Highly photofunctional and selectively biointeractive clusters would be valuable tools for the non-covalent labeling of proteins and cell-surfaces under fluorescent microscopy, and potentially useful as sensors for specific proteins.

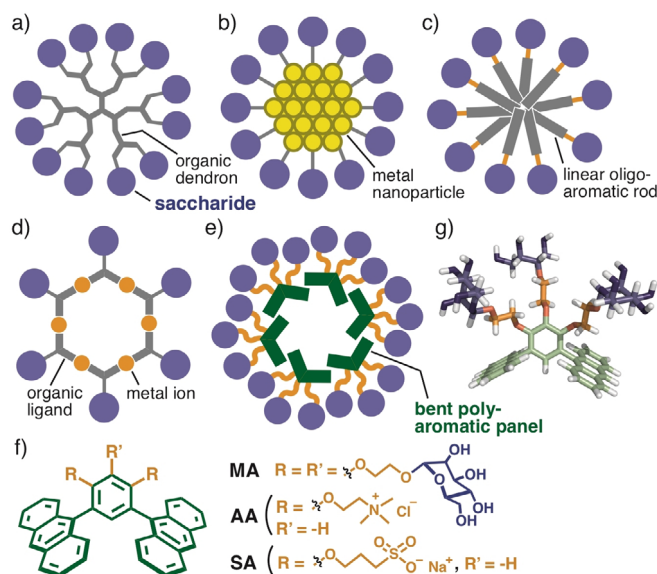


Figure 1. a) Dendrimer-shaped, b) metal nanoparticle-based, c) micellar, and d) MOF-type saccharide clusters, and e) a new saccharide cluster based on an aromatic micelle. f) Bent amphiphile **MA** with mannose groups, designed herein, and **AA** and **SA** reported previously. g) Optimized structure of **MA**.

For the design of a novel saccharide cluster with strong and changeable fluorescent color, we took inspiration from an aromatic micelle, composed of bent polyaromatic amphiphiles **AA** with hydrophilic ammonium groups on the convex side (Figure 1 f).^[11] The rational replacement of the two ionic substituents with three monosaccharide groups generates an aqueous multisaccharide-coated aromatic micelle possessing a polyaromatic cavity (Figure 1 e), yielding a novel saccharide cluster with the desired photofunctions. This marks the first synthetic success to decorate aromatic micelles with biofunctional groups and the first elucidation of their interactions with proteins *in vitro*, as part of our ongoing efforts towards biocompatible nanocontainers.^[12]

Here we report the synthesis of bent polyaromatic amphiphile **MA** with three mannose-based pendants (Figure 1 f,g) and the quantitative formation of new multimannose-coated aromatic micelle (**MA**)_n in water. The present saccharide cluster displays the following five features: 1) the spherical polyaromatic core (ca. 2 nm in diameter) is surrounded by ca. 18 mannose groups; 2) the self-assembled structure is stable enough under high dilution conditions (up to 0.02 mM based on **MA**); 3) cluster (**MA**)_n emits blue fluorescence with moderate quantum yield ($\Phi_F = 19\%$); 4) the emission color can be altered to strong red, orange, and green ($\Phi_F = 41\text{--}67\%$) upon encapsulation of fluorescent dyes

[*] H. Narita, Prof. Dr. M. Yoshizawa
Laboratory for Chemistry and Life Science, Institute of Innovative Research, Tokyo Institute of Technology
4259 Nagatsuta, Midori-ku, Yokohama 226-8503 (Japan)
E-mail: yoshizawa.m.ac@m.titech.ac.jp

Dr. L. Catti
WPI Nano Life Science Institute, Kanazawa University
Kakuma-machi, Kanazawa 920-1192 (Japan)

Supporting information and the ORCID identification number(s) for the author(s) of this article can be found under:
<https://doi.org/10.1002/anie.202102547>.

(e.g., squaraines, rubrene, and coumarins), without typical covalent functionalization; 5) selective interactions are found between mannose-binding proteins (i.e., concanavalin A) and the clusters with/without fluorescent dyes.

Mannose-attached amphiphile **MA** was synthesized in two steps from our bent building block^[12] and the quantitative formation of mannose cluster (**MA**)_n in water was revealed by NMR, DLS, and AFM analyses. Etherification of 1,5-di(9-anthryl)-2,3,4-trihydroxybenzene with a tetra-*O*-acetylmannose derivative (39% yield) and subsequent deprotection (84% yield) gave rise to **MA**.^[13,14] Stirring a suspension of **MA** (0.4 mg, 0.4 μmol) in D₂O (0.4 mL) at 100 °C for 30 min resulted in a clear, colorless solution including cluster (**MA**)_n. Whereas the ¹H NMR spectrum of **MA** in CD₃OD showed five sharp aromatic signals and complicated mannose signals in the ranges of 8.5–6.9 and 4.9–3.0 ppm, respectively, that of the product in D₂O was extremely broadened (Figure 2a,b). The broad signals sharpen at elevated temperatures (e.g., 60 °C, Figure 2c), suggesting that the motion of the polyaromatic panels of **MA** is restricted in the assembled state on the NMR timescale.^[15] The selective formation of well-defined cluster (**MA**)_n (*n* = ca. 6) was confirmed by particle size analyses. The DLS chart of (**MA**)_n in water indicated the formation of small particles with an average polyaromatic-core diameter of ca. 2 nm (Figure 2d). The AFM image of (**MA**)_n on mica displayed the presence of spherical particles with an average outer shell diameter of 2.6 ± 0.6 nm (Figure 2e,f). Molecular modeling studies suggested the dominant formation of a spherical hexamer of **MA** (Figure 2g), whose core and outer diameters (i.e., 1.9 and 3.1 nm) are comparable to those of the DLS and AFM data, respectively. The partially

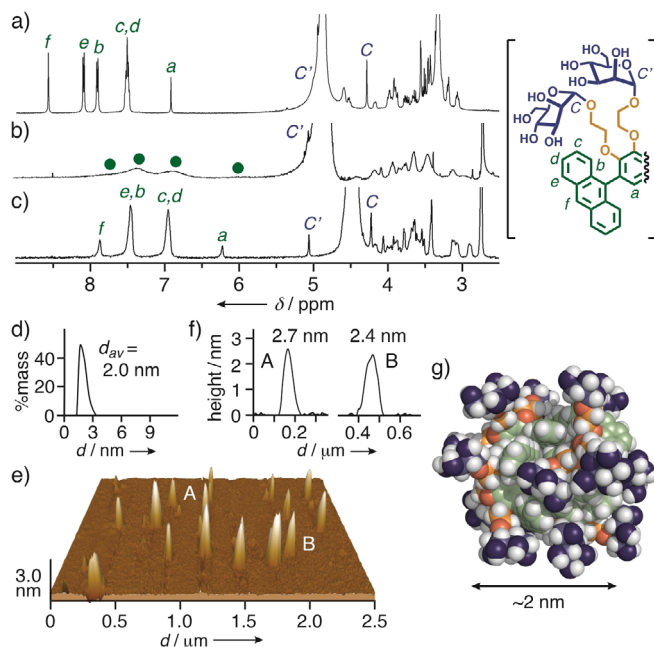


Figure 2. ¹H NMR spectra (500 MHz, 1.0 mM based on **MA**) of a) **MA** in CD₃OD and b) (**MA**)_n in D₂O at r.t., and c) (**MA**)_n in D₂O at 60 °C. d) DLS chart (r.t., H₂O, 0.1 mM based on **MA**) of (**MA**)_n. e) AFM image (r.t., dry, mica) of (**MA**)_n, and f) the selected height profiles. g) An optimized structure of (**MA**)₆.

stacked polyaromatic core of (**MA**)₆ is thoroughly coated by 18 mannose-based pendants.

Spectroscopic analyses of (**MA**)_n revealed its moderate emissivity and relatively high stability against low concentration. The UV/Vis absorption bands of (**MA**)_n in H₂O were slightly red-shifted ($\Delta\lambda_{\max} = +5$ nm) relative to those of **MA** in CH₃OH, implying anthracene-based π -stacking interactions (Figure 3a). The emission bands of (**MA**)_n were

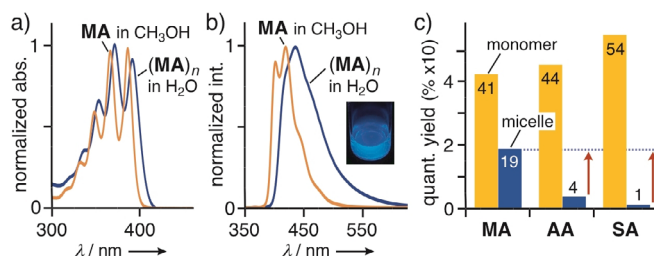


Figure 3. a) UV/Vis spectra (r.t., 0.1 mM based on **MA**) of (**MA**)_n in H₂O and **MA** in CH₃OH and, b) their fluorescence spectra ($\lambda_{\text{ex}} = 366$ nm). c) Fluorescence quantum yields (r.t., $\lambda_{\text{ex}} = 366$ nm) of **MA**, **AA**, and **SA** in the monomeric (CH₃OH, 0.1 mM) and micellar states (H₂O, 0.1 or 1.0 mM based on the monomers).

observed at $\lambda_{\max} = 435$ nm with apparent red-shifts ($\Delta\lambda_{\max} = +17$ nm) and broadening, as compared with those of **MA** (Figure 3b).^[16] The fluorescent quantum yields (Φ_F) of (**MA**)_n and **MA** were estimated to be 19 and 41%, respectively (Figure 3c). Notably, the Φ_F of (**MA**)_n is 5- and 19-times higher than that of analogous micelles (**AA**)_n and (**SA**)_n with ionic substituents, respectively (Figure 3c).^[13] The observed, enhanced emission of (**MA**)_n most probably stems from restricted π -stacking interactions between the polyaromatic panels,^[17] owing to the sterically hindered saccharide groups. The concentration-dependent emission study in water indicated the critical micelle concentration (CMC) of **MA** being 0.02 mM (Figure S23), which is ca. 50 times smaller than that of (**AA**)_n.^[11] The observed, increased stability of (**MA**)_n against dilution is derived from the non-repulsive, nonionic hydrophilic groups.

Emission color and intensity of (**MA**)_n could be altered upon encapsulation of various water-insoluble fluorescent dyes, through mainly the hydrophobic effect in water. Such facile, non-covalent modifications have been rarely demonstrated with the previous covalent and non-covalent clusters.^[9] For instance, red-fluorescent saccharide clusters were readily prepared employing hydrophobic squaraine dye **Squ** and dicyanomethylenepyran dye **DCM**. When a mixture of **MA** (0.2 mg, 0.2 μmol) and **Squ** (0.01 equiv) was manually ground for 1 min, followed by sequential water addition (2.0 mL), centrifugation, and filtration, a clear aqueous solution of (**MA**)_n-(**Squ**)_m in pale blue was obtained (Figure 4a,b).^[18] The host-guest structure was confirmed by the UV/Vis spectrum, where a new absorption band derived from encapsulated (**Squ**)_m was observed at 684 nm (Figure 4c). The DLS analysis indicated the selective formation of small particles with a core diameter of 2.1 nm, implying the presence of (**MA**)₆-**Squ** (Figure S28 and S29).

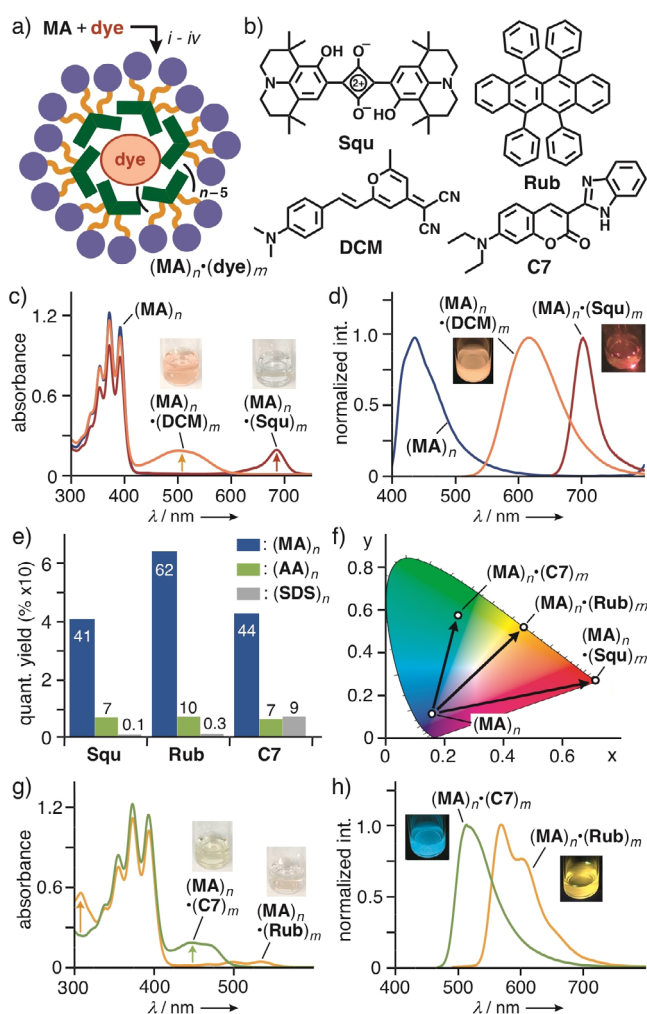


Figure 4. a) Preparation of clusters $(MA)_n \cdot (dye)_m$ with various emission colors, through (i) grinding, (ii) water addition, (iii) centrifugation, and (iv) filtration. b) Fluorescence dyes studied herein. c) UV/Vis spectra (H_2O , r.t., 0.1 mM based on MA) of $(MA)_n$ and $(MA)_n \cdot (DCM \text{ or } Squ)_m$, and d) their fluorescence spectra ($\lambda_{ex} = 366, 500,$ and 680 nm, respectively). e) Fluorescence quantum yields (H_2O , r.t., 0.1 or 1.0 mM based on the monomers) of $(MA)_n$, $(AA)_n$, and $(SDS)_n$ including Squ , Rub , and $C7$ dyes. f) CIE chromaticity diagram of $(MA)_n \cdot (dye)_m$. g) UV/Vis spectra (H_2O , r.t., 0.1 mM based on MA) of $(MA)_n \cdot (Rub \text{ or } C7)_m$ and h) their fluorescence spectra ($\lambda_{ex} = 465$ and 440 nm, respectively).

Complex $(MA)_n \cdot (Squ)_m$ exhibited strong red emission ($\Phi_F = 41\%$) with a sharp band ($\lambda_{max} = 702$ nm) upon irradiation at 680 nm (Figure 4d). In contrast, host-guest complexes $(AA)_n \cdot (Squ)_m$ and $(SDS)_n \cdot (Squ)_m$,^[13] prepared by the same protocol using amphiphiles AA or SDS and Squ , showed weak emission ($\Phi_F = 7$ and 0.1% , respectively; Figure 4e). Therefore, the facile preparation and intense emission of new fluorescent saccharide clusters were simultaneously accomplished by the present system. The CIE chromaticity diagram clarified the distinct change in the emission color of $(MA)_n$ from blue ($x, y = 0.16, 0.12$) to red ($x, y = 0.74, 0.27$) upon encapsulation of Squ (Figure 4f). Stronger red emission ($\lambda_{max} = 617$ nm, $\Phi_F = 55\%$) was generated from an aqueous pale red solution of $(MA)_n \cdot (DCM)_m$, prepared from MA and DCM by the grinding method, upon

irradiation at 500 nm (Figure 4c,d). The nonionic and sterically demanding features of the hydrophilic substituents effectively enhanced emissivity of the present multisaccharide-coated host-guest complexes, via the suppression of usual ACQ, found in micelles $(AA)_n$ and $(SDS)_n$ (Figure 4e).

In the same way, strong orange and green fluorescent clusters were also obtained in water by the treatment of $(MA)_n$ with rubrene (Rub) and coumarin 7 ($C7$), respectively. The obtained, pale red solution of $(MA)_n \cdot (Rub)_m$ displayed broad absorption bands in the range of 430 to 580 nm and fluorescence bands at $\lambda_{max} = 558$ nm with high quantum yield ($\Phi_F = 62\%$), corresponding to the encapsulated $(Rub)_m$ (Figure 4g,h). Interestingly, the encapsulation efficiency and Φ_F of $(MA)_n \cdot (Rub)_m$ are 2.0- and 6.1-times higher than those of $(AA)_n \cdot (Rub)_m$ under the same conditions.^[18] Complex $(MA)_n \cdot (C7)_m$ emitted green fluorescence with good quantum yield ($\Phi_F = 44\%$, respectively; Figure 4e,h). The orange and green emissions were quantified by the CIE diagram (Figure 4f).

Finally, multimannose cluster $(MA)_n$ and its host-guest complex exhibited selective interaction abilities toward the outer surface of a mannose-binding protein, concanavalin A ($ConA$),^[19] in water at room temperature. The multipoint surface-surface interactions can be visualized through aggregation-based colloid formation.^[9] When an aqueous solution of $(MA)_n$ (1.0 mL; 0.1 mM based on MA) was added to a clear solution of $ConA$ (2.0 mL; 0.5 mM) in HEPES buffer, the resultant solution gradually became opaque, suggesting the formation of colloidal aggregates comprising the proteins and clusters, monitored by UV/Vis turbidity analysis (Figure 5a).^[13] Upon addition of excess α -methyl mannopyranoside (MM) as an inhibitor, the opaque solution turned clear due to the dissociation of the aggregates, indicating the surface-surface interactions between $(MA)_n$ and $(ConA)_p$. The exterior mannose groups of $(MA)_n$ are essential for the interactions and accordingly analogue $(AA)_n$ showed no

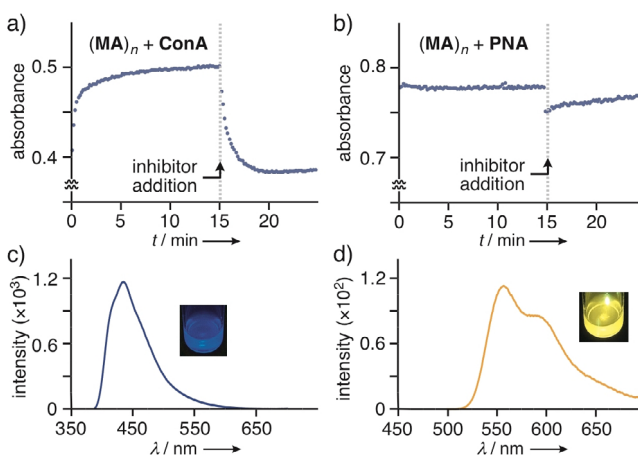


Figure 5. Turbidity measurements (H_2O , r.t., HEPES buffer, $\lambda_{det} = 366$ nm) of a) $ConA$ after addition of $(MA)_n$ (0.1 mM based on MA) and b) PNA after addition of $(MA)_n$ (0.2 mM based on MA). Inhibitor MM or D-(+)-galactose was added to the mixtures at 15 min. Fluorescence spectra (H_2O , r.t., $\lambda_{ex} = 366$ or 465 nm) and photographs ($\lambda_{ex} = 365$ or 470 nm) of cluster-protein complexes c) $(MA)_n \cdot (ConA)_p$ and d) $[(MA)_n \cdot (Rub)_m] \cdot (ConA)_p$.

aggregate formation (Figure S35).^[20] In addition, no protein-cluster interaction was observed by the treatment of $(\mathbf{MA})_n$ (0.2 mM based on \mathbf{MA}) with a galactose-binding protein (\mathbf{PNA})^[19] under similar conditions, even when using twice the amount of $(\mathbf{MA})_n$ (Figure 5b).

More importantly, the selective protein-cluster interactions were also detected with different fluorescence colors in water. Dissolved white aggregates $(\mathbf{MA})_n \cdot (\mathbf{ConA})_p$, collected from the mixed solution of $(\mathbf{MA})_n$ and \mathbf{ConA} in buffer,^[20] displayed visible blue emission ($\lambda_{\max} = 433$ nm) in water (Figure 5c). Taking advantage of the easy preparation and high stability of the multimannose-coated host-guest complexes, in the same way, orange emission ($\lambda_{\max} = 557$ nm) was detected from pale red aggregates, obtained from host-guest complex $(\mathbf{MA})_n \cdot (\mathbf{Rub})_m$ with \mathbf{ConA} , in water (Figure 5d).

In conclusion, we have developed a new type of a synthetic saccharide cluster with changeable fluorescent colors, on the basis of an aromatic micelle. In water, bent polyaromatic amphiphiles bearing three mannose groups quantitatively assembled into a spherical cluster with a 2 nm-sized polyaromatic core surrounded by ca. 18 saccharide pendants, as confirmed by NMR, DLS, and AFM analyses. The relatively stable cluster could alter its emissivity from moderate blue to strong red, orange, and green (Φ_F up to 67%) upon simple encapsulation of fluorescent dyes, without additional multi-step and time-consuming synthetic procedures as well as typical aggregation-caused quenching. Furthermore, the studies on cluster-protein interactions revealed that the multimannose cluster can selectively bind to mannose-binding proteins, which was detected by turbidity and fluorescence (two emission colors) analyses. As a future perspective, the present “aromatic micelle”-based system would facilitate the straightforward construction of a new library of multisaccharide clusters by variation of the (i) saccharide pendants, (ii) polyaromatic core frameworks,^[21] and (iii) fluorescent/phosphorescent guests, for made-to-order bioapplications (e.g., in vitro biosensors and bioimaging tags).

Acknowledgements

This work was supported by JSPS KAKENHI (Grant No. JP18H01990 and JP19H04566) and “Support for Tokyo Tech Advanced Researchers (STAR)”. L.C. thanks the JSPS and Humboldt Postdoctoral Fellowship.

Conflict of interest

The authors declare no conflict of interest.

Keywords: aromatic micelle · encapsulation · fluorescent color · host-guest complex · saccharide cluster

[1] a) Y. C. Lee, R. T. Lee, *Acc. Chem. Res.* **1995**, *28*, 321–327; b) M. Mammen, S.-K. Choi, G. M. Whitesides, *Angew. Chem. Int. Ed.* **1998**, *37*, 2754–2794; *Angew. Chem.* **1998**, *110*, 2908–2953.

[2] A. Varki, R. D. Cummings, J. D. Esko, P. Stanley, G. W. Hart, M. Aebi, A. G. Darvill, T. Kinoshita, N. H. Packer, J. H. Prestegard,

R. L. Schnaar, P. H. Seeberger, *Essentials of Glycobiology*, 3rd ed., CSH Press, New York, **2017**.

- [3] a) K. Aoi, K. Itoh, M. Okada, *Macromolecules* **1995**, *28*, 5391–5393; b) T. K. Lindhorst, C. Kieburg, *Angew. Chem. Int. Ed. Engl.* **1996**, *35*, 1953–1956; *Angew. Chem.* **1996**, *108*, 2083–2086; c) D. Zanini, R. Roy, *J. Am. Chem. Soc.* **1997**, *119*, 2088–2095.
- [4] a) T. Fujimoto, C. Shimizu, O. Hayashida, Y. Aoyama, *J. Am. Chem. Soc.* **1997**, *119*, 6676–6677; b) J. M. Benito, M. Gómez-García, C. O. Mellet, I. Baussanne, J. Defaye, J. M. García Fernández, *J. Am. Chem. Soc.* **2004**, *126*, 10355–10363; c) J. Kim, Y. Ahn, K. M. Park, Y. Kim, Y. H. Ko, D. H. Oh, K. Kim, *Angew. Chem. Int. Ed.* **2007**, *46*, 7393–7395; *Angew. Chem.* **2007**, *119*, 7537–7539; d) G. Yu, Y. Ma, C. Han, Y. Yao, G. Tang, Z. Mao, C. Gao, F. Huang, *J. Am. Chem. Soc.* **2013**, *135*, 10310–10313.
- [5] a) J. M. de la Fuente, A. G. Barrientos, T. C. Rojas, J. Rojo, J. Cañada, A. Fernández, S. Penadés, *Angew. Chem. Int. Ed.* **2001**, *40*, 2257–2261; *Angew. Chem.* **2001**, *113*, 2317–2321; b) C.-C. Lin, Y.-C. Yeh, C.-Y. Yang, C.-L. Chen, G.-F. Chen, C.-C. Chen, Y.-C. Wu, *J. Am. Chem. Soc.* **2002**, *124*, 3508–3509.
- [6] B.-S. Kim, D.-J. Hong, J. Bae, M. Lee, *J. Am. Chem. Soc.* **2005**, *127*, 16333–16337.
- [7] H.-K. Lee, K. M. Park, Y. J. Jeon, D. Kim, D. H. Oh, H. S. Kim, C. K. Park, K. Kim, *J. Am. Chem. Soc.* **2005**, *127*, 5006–5007.
- [8] a) N. Kamiya, M. Tominaga, S. Sato, M. Fujita, *J. Am. Chem. Soc.* **2007**, *129*, 3816–3817; b) J. E. M. Lewis, A. B. S. Elliott, C. J. McAdam, K. C. Gordon, J. D. Crowley, *Chem. Sci.* **2014**, *5*, 1833–1843; c) L.-J. Chen, Y.-Y. Ren, N.-W. Wu, B. Sun, J.-Q. Ma, L. Zhang, H. Tan, M. Liu, X. Li, H.-B. Yang, *J. Am. Chem. Soc.* **2015**, *137*, 11725–11735.
- [9] M. Delbianco, P. Bharate, S. Varela-Aramburu, P. H. Seeberger, *Chem. Rev.* **2016**, *116*, 1693–1752.
- [10] a) A saccharide cluster with high emissivity ($\Phi_F = 37\%$) in water: G. J. L. Bernardes, R. Kikkeri, M. Maglino, P. Laurino, M. Collot, S. Y. Hong, B. Lepenies, P. H. Seeberger, *Org. Biomol. Chem.* **2010**, *8*, 4987–4996; b) A saccharide cluster with two emission colors in water: H. Zhang, L. Zhang, R.-P. Liang, J. Huang, J.-D. Qiu, *Anal. Chem.* **2013**, *85*, 10969–10976.
- [11] a) K. Kondo, A. Suzuki, M. Akita, M. Yoshizawa, *Angew. Chem. Int. Ed.* **2013**, *52*, 2308–2312; *Angew. Chem.* **2013**, *125*, 2364–2368; b) Y. Okazawa, K. Kondo, M. Akita, M. Yoshizawa, *J. Am. Chem. Soc.* **2015**, *137*, 98–101; c) Y. Okazawa, K. Kondo, M. Akita, M. Yoshizawa, *Chem. Sci.* **2015**, *6*, 5059–5062.
- [12] a) K. Kondo, J. K. Klosterman, M. Yoshizawa, *Chem. Eur. J.* **2017**, *23*, 16710–16721; b) M. Yoshizawa, L. Catti, *Acc. Chem. Res.* **2019**, *52*, 2392–2404.
- [13] See the Supporting Information. (\mathbf{SDS})_n is a typical aliphatic micelle composed of sodium dodecyl sulfate (\mathbf{SDS}) amphiphiles.
- [14] We also synthesized an analogue of \mathbf{MA} bearing two mannose groups, which shows poor solubility in water (Figure S13–15).^[13]
- [15] The DOSY NMR spectrum of $(\mathbf{MA})_n$ (1.0 mM based on \mathbf{MA}) in D₂O at 60 °C showed a single band at a diffusion coefficient (D) of 3.8×10^{-10} m²s⁻¹ (Figure S17 and S18), which indicates the thermal stability of the self-assembled structure (2.3 nm in average diameter).
- [16] The emission lifetime analysis of \mathbf{MA} in CH₃OH and $(\mathbf{MA})_n$ in H₂O suggested the presence of shorter (6.5 ns) and longer lifetime species (5.1, 17.3, and 46.5 ns), respectively (Figure S22b).
- [17] a) T. Hayashi, N. Mataga, Y. Sakata, S. Misumi, M. Morita, J. Tanaka, *J. Am. Chem. Soc.* **1976**, *98*, 5910–5913; b) S. Sekiguchi, K. Kondo, Y. Sei, M. Akita, M. Yoshizawa, *Angew. Chem. Int. Ed.* **2016**, *55*, 6906–6910; *Angew. Chem.* **2016**, *128*, 7020–7024.
- [18] The uptake of fluorescent dyes with pre-made cluster $(\mathbf{MA})_n$ by stirring is less effective than the grinding protocol, due to the high kinetic barrier of hydrophobic guest incorporation into the

tightly self-assembled host framework surrounded by multiple hydrophilic groups in water. The encapsulation efficiency and Φ_F of $(\mathbf{MA})_n \cdot (\mathbf{Rub})_m$ were 31- and 205-times higher than those of $(\mathbf{SDS})_n \cdot (\mathbf{Rub})_m$ (Figure 4e and S26).^[13] Strong green fluorescence ($\Phi_F = 67\%$) was also observed from $(\mathbf{MA})_n \cdot (\mathbf{PMB})_m$, composed of \mathbf{MA} and pentamethyl boron-dipyrromethene \mathbf{PMB} (Figure S30).

- [19] a) J. H. Naismith, C. Emmerich, J. Habash, S. J. Harrop, S. R. Helliwell, W. N. Hunter, K. Raftery, A. J. Kalb, J. Yariv, *Acta Crystallogr. Sect. D* **1994**, *50*, 847–858; b) R. Banerjee, K. Das, R. Ravishan-kar, K. Suguna, A. Surolia, M. Vijayan, *J. Mol. Biol.* **1996**, *259*, 281–296.
- [20] a) No interaction of \mathbf{ConA} with monomeric \mathbf{MA} (0.1 μM) was detected under similar conditions (Figure S35f); b) The self-assembled structure of $(\mathbf{AA})_n$ is stable at low concentration (0.1 mM based on \mathbf{AA}) in the present buffer solution, as confirmed by the NMR and fluorescence analyses (Figure S37); c) According to UV/Vis analysis, 54% of initial \mathbf{MA} is consumed for the formation of precipitated aggregate $(\mathbf{MA})_n \cdot (\mathbf{ConA})_p$ after standing at room temperature for 4.5 h (Figure S36c).
- [21] a) M. Kishimoto, K. Kondo, M. Akita, M. Yoshizawa, *Chem. Commun.* **2017**, *53*, 1425–1428; b) L. Catti, N. Kishida, T. Kai, M. Akita, M. Yoshizawa, *Nat. Commun.* **2019**, *10*, 1948; c) Y. Satoh, L. Catti, M. Akita, M. Yoshizawa, *J. Am. Chem. Soc.* **2019**, *141*, 12268–12273; d) M. Hanafusa, Y. Tsuchida, K. Matsumoto, K. Kondo, M. Yoshizawa, *Nat. Commun.* **2020**, *11*, 6061; e) K. Ito, T. Nishioka, M. Akita, A. Kuzume, K. Yamamoto, M. Yoshizawa, *Chem. Sci.* **2020**, *11*, 6752–6757; f) K. Kudo, T. Ide, N. Kishida, M. Yoshizawa, *Angew. Chem. Int. Ed.* **2021**, <https://doi.org/10.1002/anie.202102043>; *Angew. Chem.* **2021**, <https://doi.org/10.1002/ange.202102043>; g) Y. Tsuchida, K. Aratsu, S. Hiraoaka, M. Yoshizawa, *Angew. Chem. Int. Ed.* **2021**, <https://doi.org/10.1002/anie.202101453>; *Angew. Chem.* **2021**, <https://doi.org/10.1002/ange.202101453>.

Manuscript received: February 19, 2021

Revised manuscript received: March 11, 2021

Accepted manuscript online: March 13, 2021

Version of record online: ■■■■■, ■■■■■

Communications

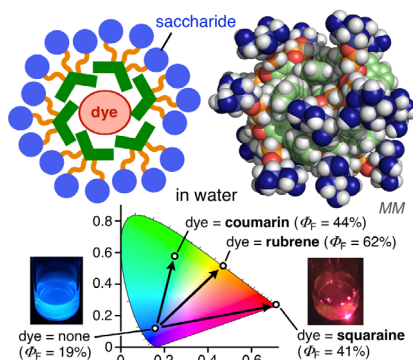


Saccharide Clusters

H. Narita, L. Catti,

M. Yoshizawa*                                        

An Aromatic Micelle-Based Saccharide Cluster with Changeable Fluorescent Color and its Protein Interactions



A multisaccharide-coated aromatic micelle forms in water through quantitative assembly of bent polyaromatic amphiphiles bearing three mannose groups. The emission intensity and color of the saccharide cluster can be altered from blue to strong red, orange, and green (Φ_F up to 67%) upon encapsulation of hydrophobic fluorescent dyes. Moreover, the present fluorescent clusters display selective interactions with mannose-binding proteins *in vitro*.